Finite Element Thermo-Structural Methodology for Investigating Diesel Engine Pistons with Thermal Barrier Coating

SAE INTERNATIONAL

ARTICLE INFO

Article ID: 03-12-01-0006

doi:10.4271/03-12-01-0006

Finite Element Thermo-Structural Methodology for Investigating Diesel Engine Pistons with Thermal Barrier Coating

Paolo Baldissera and Cristiana Delprete, *Politecnico di Torino, Italy*

Abstract

Traditionally, in combustion engine applications, metallic materials have been widely employed due to their properties: castability and machinability with accurate dimensional tolerances, good mechanical strength even at high temperatures, wear resistance, and affordable price. However, the high thermal conductivity of metallic materials is responsible for consistent losses of thermal energy and has a strong influence on pollutant emission.
A possible approach for reducing the thermal exchange requires the use of thermal barrier coating (TBC) made by materials with low thermal conductivity and good thermo-mechanical strength.

In this work, the effects of a ceramic coating for thermal insulation of the piston crown of a car diesel engine are investigated through a numerical methodology based on finite element analysis. The study is developed by considering firstly a thermal analysis and then a thermo-structural analysis of the component. The loads acting on the piston are considered both separately and combined to achieve a better understanding of their mutual interaction and of the coating effect on the stress state.

The thermal analysis pointed out a decrease of temperature up to 40°C in the upper part of the piston for the coated model. Despite the lower deformations induced by the reduced thermal load, the stiffening effect provided by the TBC results in higher peak stress. However, the lower temperature field inside the piston compensates by allowing higher yielding stresses for the component and reducing the impact on the safety factor.

The methodology is validated by comparison of the model results with numerical data available from the literature; limitations and potential future improvements are also discussed.

History

Received: 09 Apr 2018
Revised: 14 Jul 2018
Accepted: 23 Aug 2018
e-Available: 14 Dec 2018

Keywords

FEM, Mechanical components, Numerical method, Piston, Thermal barrier coating, TBC, Thermo-structural analysis

Citation

Baldissera, P. and Delprete, C., "Finite Element Thermo-Structural Methodology for Investigating Diesel Engine Pistons with Thermal Barrier Coating," *SAE Int. J. Engines* 12(1):2019, doi:10.4271/03-12-01-0006.

ISSN: 1946-3936
e-ISSN: 1946-3944

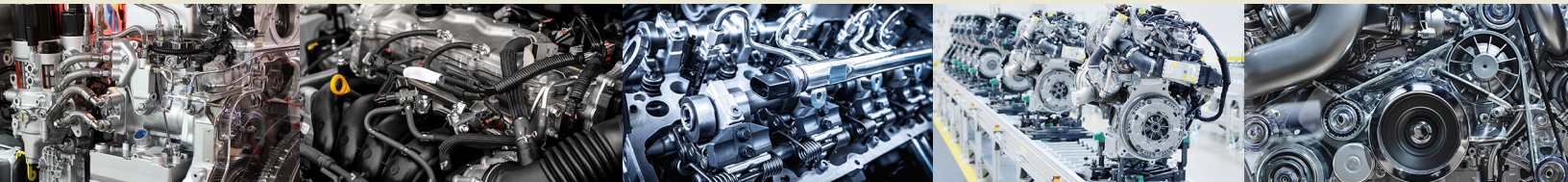

Introduction

The constant development of new technologies in many engineering fields requires an advanced knowledge about materials since the beginning of the design phase. Nowadays, the market offers a wide range of new materials that can answer the engineer requirements for a continuous product improvement.

Traditionally, in combustion engine applications, metallic materials have been widely employed due to their properties: castability and machinability with accurate dimensional tolerances, good mechanical strength even at high temperatures, wear resistance, and affordable price. However, the high thermal conductivity of metallic materials is responsible for consistent losses of thermal energy and has a strong influence on pollutant emission.

The development of low heat rejection engines (LHRE) started back in the 1970s and is again a key topic in the current scenario. The survival of the internal combustion engine technology, under the increasing pressure of emission standard requirements and with the rise of hybrid and electric car technologies, is strongly related to the ability of engineers to evolve toward higher efficiency and lower emissions. LHRE development includes a better insulation of the combustion chamber, an effective reduction of the friction losses between the piston and the cylinder, a decrease of the inertia in the turbine housing, and exhaust energy recovery systems.

Thermal losses at the combustion chamber represent a significant fraction of the overall vehicle losses [1]. By studying a diesel engine in steady-state conditions (4 bar of mean effective pressure at 1500 rpm), the thermal flux distribution was investigated in [2] by means of thermocouples. As a result, the thermal exchange through each component of the combustion chamber has been quantified. The thermal flux can reach 10 MW/m^2 during the combustion process [3], and the resulting temperature fluctuations can lead to degradation of mechanical properties for critical components such as the piston, the cylinder, and the valves.

Many experimental studies were conducted to achieve a better understanding of the mechanisms affecting the thermal exchange in the combustion chamber. The main factors are engine working load and speed, compression ratio, supercharging level, exhaust gas recirculation (EGR) level, ignition advance, and fluid motion inside the cylinder [4]. Controlling these factors can be the key to decrease thermal losses and to reduce thermal loads on engine components.

Another approach for reducing the thermal exchange can be the insulation of engine components that are directly in touch with combustion gases. This can be obtained through the so-called thermal barrier coating (TBC) made by materials with low thermal conductivity and good thermo-mechanical strength [5]. Ceramics and polymeric coatings developed during the last decades offer a good potential for innovation in this perspective, but still they must be evaluated both from economical and performance point of views.

The development of gasoline LHRE was stopped by the risk of autoignition due to the higher temperatures reached in the combustion chamber [6, 7]. For this reason, the LHRE research moved toward diesel engines but with conflicting results. On the one hand, zirconia and other ceramic TBC on piston crown, cylinder head, and valves showed a reduction from 30% to 80% in both peak and average thermal flux [8, 9, 10, 11, 12]. On the other hand, pistons insulated by thick TBC have shown up to 100% increase in peak thermal flux that was attributed to the rise of thermal exchange coefficients due to higher temperatures on the boundary surfaces [13, 14]. Other researchers observed fuel consumption increases and reduced thermal efficiency that were ascribed to a degradation of the combustion reaction [15]. Many authors substantially agree that, to achieve benefits from ceramic coatings, a specific optimization of the injection timing is required [11, 12, 13, 14, 15, 16]. More encouraging results were achieved with thinner ceramic coatings (below 1 mm), with less drawbacks: fuel consumption was slightly reduced (from 1% to 9%) in turbo-compressed diesel engines by introduction of a 0.30-0.35 mm ceramic coating on piston crown and cylinder head [17, 18, 19].

In this work, a methodology is presented on a case study piston model based on available literature data, not linked to a specific market product. The effects of a ceramic coating for thermal insulation of the piston crown of a car diesel engine are investigated through finite element analysis (FEA). The purpose is to define a methodology to evaluate the potential benefit in terms of thermal load reduction leading to structural improvement of the component.

Materials and Methods

Piston Base Materials

The considered piston material is an aluminum alloy AlSi12Cu3MgNi having the mechanical and thermo-physical properties summarized in Tables 1 and 2 as function of the working temperature, with some exceptions assumed as constant.

The alfin material is a Ni-resist cast iron, whose properties are summarized in Tables 3 and 4.

TABLE 1 Thermo-physical properties of the piston AlSi12Cu3MgNi alloy.

T [°C]	ρ [kg m^{-3}]	λ [W m^{-1} K^{-1}]	α [10^{-6} °C^{-1}]	c_p [J kg^{-1} K^{-1}]
20	2700	155.0	21.5	963
100	2700	155.2	22.1	963
150	2700	156.0	22.4	963
200	2700	157.3	22.8	963
250	2700	159.0	23.1	963
300	2700	161.2	23.5	963
350	2700	164.0	23.9	963

TABLE 2 Mechanical properties of the piston AlSi12Cu3MgNi alloy.

T [°C]	E [MPa]	ν [-]	$\sigma_{0.2\,true}$ [MPa]	UTS_{true} [MPa]
20	80,000	0.33	211	228
150	77,300	0.33	201	209
250	72,500	0.33	90	130
350	65,000	0.33	25	60
430	60,000	0.33	20	46

TABLE 3 Thermo-physical properties of the alfin Ni-resist cast iron.

T [°C]	ρ [kg m^{-3}]	λ [W m^{-1} K^{-1}]	α [10^{-6} °C^{-1}]	c_p [J kg^{-1} K^{-1}]
20	7450	32	12.3	460

TABLE 5 Thermo-physical properties of the 8YSZ applied through APS as given by [21, 22, 23, 24] or interpolated through linear* or logarithmic** regression.

T [°C]	ρ [kg m^{-3}]	λ [W m^{-1} K^{-1}]	α [10^{-6} °C^{-1}]	c_p [J kg^{-1} K^{-1}]
25	5100	1.72	7.81*	334.6**
75	5239*	1.81**	7.87*	427.8
100	5309*	1.83	7.90	456.8**
125	5378*	1.86**	7.93*	476.2
250	5726*	1.95**	8.09*	544.4
300	5865*	1.95	8.15*	553.6**
500	6422*	1.97	8.40	601.4
600	6700	2.00**	8.53*	614.6**
700	6978*	2.01	8.65*	628.2**
750	7117*	2.02**	8.71*	628.4

Selected TBC Properties

The most important properties affecting the choice of a ceramic coating for the piston crown are:

- High melting temperature
- Low thermal conductivity
- Affinity with the substrate material with respect to the thermal expansion coefficient, to grant adhesion
- High mechanical strength at high temperature
- Good resistance to erosion and corrosion
- No phase changes from ambient to operating condition temperatures
- Chemical stability to avoid reactions with fuel mixture or exhausts
- Low sintering rate of the porous microstructure
- Fatigue resistance at both low and high cycles
- Toughness
- Low specific weight
- Low cost

The coating porosity affects both its thermal conductivity and elastic modulus. For a TBC with lower thermal expansion coefficient, it is better to have a lower elastic modulus for a durable coating [20].

To perform a thermo-structural analysis, it is important to consider temperatures and thermal fluxes that the piston has to undergo during its working cycle. The piston crown is directly exposed to the combustion process, which is not uniform and leads to different temperature distributions in both radial and circumferential directions. Therefore, the piston crown shows a distribution of different thermal exchange coefficients on its surface.

The heat generated by the combustion reaches the piston crown by convection (plus a contribution from radiation) and is transmitted by conduction inside the piston body, generating stresses and strains. A TBC on the piston crown can limit the amount of transmitted heat with a reduction of the thermal-generated mechanical stresses. The mass of the piston is mainly distributed around the pin housing area, and so higher deformations are present in this zone.

Typical TBCs consist of a top layer and a bond coat. The first one is a ceramic coating with a thickness of about 300 µm, usually applied through atmospheric plasma spray (APS). The second one is usually a MCrAlY (where M can be Ni or Co) with a thickness of 100 µm, generated through vacuum plasma spray (VPS).

In the present work, the effects of 8YSZ TBC with a bond layer of NiCrAlY on the piston crown are analyzed. The 8YSZ is a dense coating with 8%mol of Y_2O_3 and its thermo-physical and mechanical properties are shown in Tables 5 and 6, respectively. The missing values for the specific weight ρ and for the thermal expansion coefficient α were estimated by linear regression. A logarithmic regression was used to give the best fitting over literature data ($R^2 > 0.99$) for the thermal

TABLE 4 Mechanical properties of the alfin Ni-resist cast iron.

T [°C]	E [MPa]	ν [-]	$\sigma_{0.2\,true}$ [MPa]	$\sigma_{R,\,true}$ [MPa]
20	170,000	0.28	150	194
100	170,000	0.28	150	174
150	170,000	0.28	141	163
400	170,000	0.28	130	153

TABLE 6 Mechanical properties of the 8YSZ applied through APS as given by [25] or interpolated through second-degree polynomial* regression.

T [°C]	E [GPa]	ν [-]	σ_{lim} [MPa]
20	62.5	0.25	800
100	59.6	0.25	725*
300	50.3*	0.25	560
500	37.5*	0.25	450
600	29.8	0.25	390

FIGURE 1 Logarithmic regression on λ and c_p values for the 8YSZ.

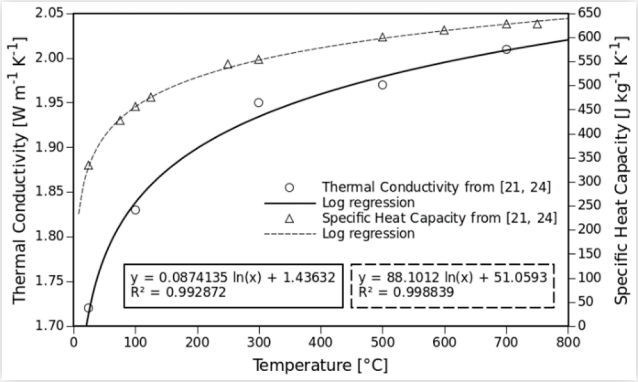

conductivity λ and for the specific heat capacity c_p to extrapolate the missing values (Figure 1). Since the 8YSZ is ceramic, its mechanical behavior should be fragile. However, plasma sprayed ceramics usually show a nonlinear behavior due to coalescence of micro-cracks and micro-pores. For the purpose of this study, the onset of these phenomena are considered as limit. The missing values for the elastic modulus E and for the limit strength (σ_{lim}) were obtained through a second-degree polynomial regression (Figure 2), while Poisson's ratio was assumed as independent from the temperature.

The thermo-physical and the mechanical properties of the NiCrAlY bond layer are reported in Tables 7 and 8, respectively.

Finite Element Modeling

The finite element discretization was obtained in Hypermesh® as summarized in Table 9 and shown in Figure 3. In the following, "model A" will refer to the uncoated piston, while "model B" will be used to indicate the coated one.

FIGURE 2 Polynomial regression on E and UTS values for the 8YSZ.

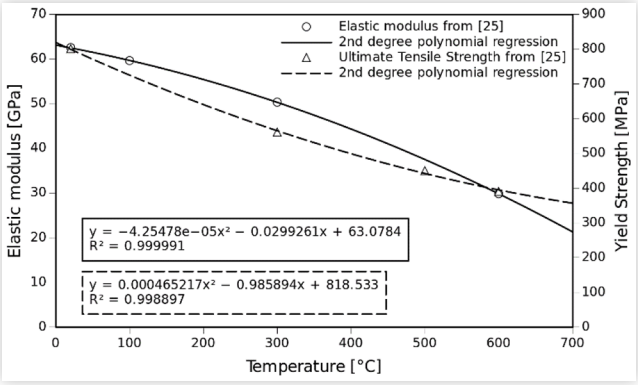

TABLE 7 Thermo-physical properties of the NiCrAlY [21, 26].

T [°C]	ρ [kg m^{-3}]	λ [W m^{-1} K^{-1}]	α [10^{-6} °C^{-1}]	c_p [J kg^{-1} K^{-1}]
20	8050	10.0	7.2	450
900	8050	24.0	16.9	676

TABLE 8 Mechanical properties of the NiCrAlY [27].

T [°C]	E [MPa]	ν [-]	$\sigma_{0.2\ true}$ [MPa]	UTS_{true} [MPa]
20	225,000	0.3	501	952
800	147,000	0.3	191	638

The TBC+bond layer was added to model B through a 0.4 mm thin layer of wedge elements, extruded in normal direction from the piston crown element faces. As first approximation, the material properties of such layer were assigned as weighted average between the 8YSZ TBC and the NiCrAlY bond, by using the respective thickness (0.3 and 0.1 mm) as weighting factors.

Finite Element Simulation

Two simulations were conducted on both A and B models:

1. A thermal analysis to evaluate the coating effects on temperature distribution across the piston
2. A thermo-structural analysis to evaluate the stress and strain state caused by the combined thermal and mechanical loads with and without TBC

The following assumptions and simplifications were made:

- Pure convective thermal exchange on the piston: the gas radiative component and the skirt-cylinder conductive component were both neglected.
- Engine steady-state condition: maximum load and 4300 rpm, thermal transients at engine start and during load changes are neglected.
- Piston steady-state condition at the top dead center (TDC), where maximum load and temperature are imposed by the combustion.
- Negligible lateral forces between the cylinder and the piston as well as the corresponding friction forces.
- Negligible actions from the ring pack on the piston stress state.

TABLE 9 Tetragonal mesh of the piston assembly starting model.

Component	Element type	# Nodes	# Elements
Piston	C3D10M (Tetra10)	360505	229028
Coating	C3D15 (Wedge15)	32036	7014
Alfin	C3D10M (Tetra10)	31604	16089
Pin	C3D10M (Tetra10)	55882	34756
Bushing	C3D4 (Tetra4)	3168	9108
Crank	C3D4 (Tetra4)	5742	22606

FIGURE 3 Section view of the piston assembly mesh for the coated model.

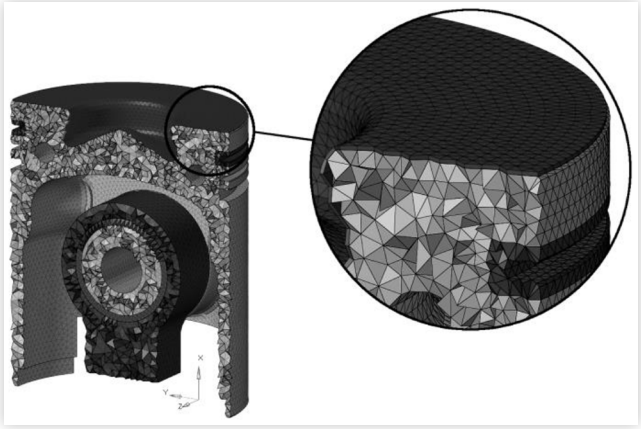

FIGURE 4 Piston macro-zones designation for the FE model.

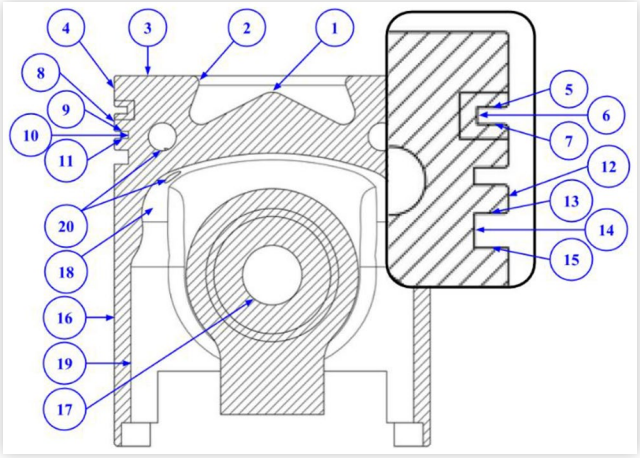

- Possible residual stresses in the coating were neglected.
- Thermal exchange properties and conditions were modeled through a finite number of macro-zones along the piston surface, instead of considering a continuous variation.

The last assumption was made in analogy to the procedure adopted in [28, 29]. Gas temperature boundary conditions and thermal exchange coefficients for each macro-zone, adopted from [28, 29], are reported in Table 10 with reference to Figure 4.

For the thermo-structural analysis, the temperature field obtained from the thermal analysis was combined to a pressure of 150 bar on the piston crown and on the top land (the piston skirt surface above the first ring). The peak pressure would be not exactly at the TDC but in the final part of the compression phase at 9° of crank angle. Since this corresponds to 3° of connecting rod obliquity (sin 3° = 0.052), the assumption of negligible lateral forces is acceptable.

TABLE 10 Heat transfer coefficients and gas temperature of piston macro-zones as referenced in Figure 4, adapted from [28, 29].

#	Macro-zone	h [W m^{-2} °C^{-1}]	T_{gas} [°C]
1	Bowl	700	741
2	Bowl edge	700	741
3	Crown	700	741
4	Top land	500	225
5	Alfin housing top surface	500	200
6	Alfin housing lateral surface	400	200
7	Alfin housing bottom surface	400	200
8	Ring land 2	400	180
9	Ring 2 housing top surface	450	180
10	Ring 2 housing lateral surface	400	180
11	Ring 2 housing bottom surface	400	180
12	Ring land 3	400	170
13	Ring 3 housing top surface	450	160
14	Ring 3 housing lateral surface	400	160
15	Ring 3 housing bottom surface	400	160
16	Piston skirt	1500	110
17	Wrist pin inner surface	1500	90
18	Piston inner top surface	1500	110
19	Piston inner bottom surface	1500	110
20	Cooling gallery	1500	130

Results and Discussion

Thermal Analysis

The number of nodes for each FE model is reported in Table 11 with the CPU and clock time for thermal analysis on two quad-core CPUs.

The temperature distribution across the piston is shown in Figure 5(a) and (b) for the uncoated and coated piston, respectively. Isothermal lines show a typical concentric trend on the piston crown as direct consequence of the assigned macro-zones and of the piston shape.

The crown temperature affects the temperature of all the underlying body. In a direct injection diesel engine, the highest temperature is at the bowl edge: here, the model estimates 282°C for the uncoated piston and 313°C for the coated one. As expected, the thermal barrier provided by the coating reduces the heat flow resulting in higher temperatures inside the combustion chamber and on the external surface of the coating. As shown in Figure 6, the properties of the TBC determine a temperature fall of 45°C across its thickness of 0.4 mm. Therefore, the rest of the coated piston body is working at a

TABLE 11 FE model size and thermal simulation time.

Model	# of nodes	CPU time	Clock time (8 cores)
A	394168	38′23″	7′13″
B	465810	46′44″	8′35″

FIGURE 5 Temperature distribution across the uncoated (a) and TBC-coated (b) piston models.

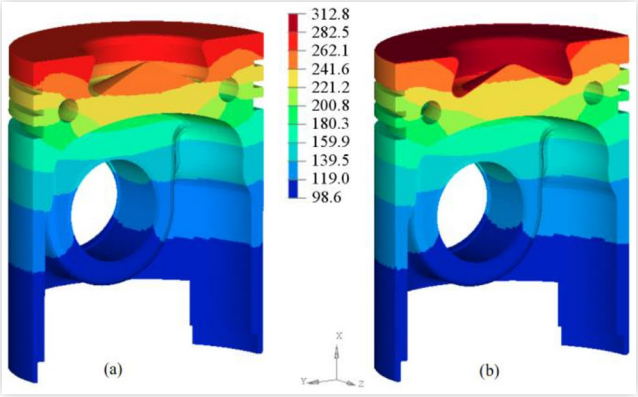

lower temperature with respect to the uncoated one. This is evident, in particular, for the core of the material, far from the unchanged thermal exchange of the skirt. The temperature profile along the piston skirt is shown in Figure 7, where it is evident there is a temperature drop of about 160°C from the crown to the end of the skirt. Such thermal field on the skirt is an important input to be considered during the piston design phase to obtain the desired coupling tolerances with the liner in working conditions.

As general validation of the analysis, a third model, uncoated and without cooling gallery, has been simulated (Figure 8) and compared to the results shown in [29]. The slight difference in temperature values can be ascribed to the different piston geometry and material properties. However, the general trend and temperature profile shows a good agreement and provides confirmation of the validity of the proposed methodology.

FIGURE 6 Temperature profile on the piston crown surface, compared with the same profile above and below the TBC for the coated model.

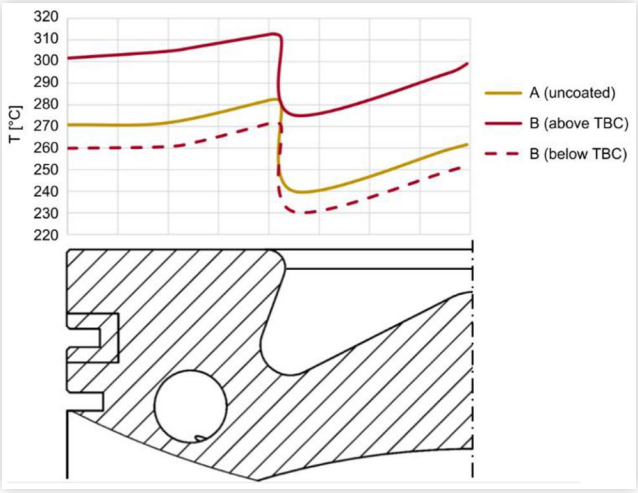

FIGURE 7 Calculated temperature profile along the piston skirt.

Thermo-Structural Analysis

In a first phase, three thermo-structural simulations were performed by applying each load condition separately (gas pressure, inertial forces, and thermal loads) in order to evaluate their individual contributions. Then, a final simulation includes all the conditions applied simultaneously.

The overall number of nodes for each model is reported in Table 12 as far as the CPU and clock time for the final thermo-structural analysis on two quad-core CPUs.

As expected, despite the relatively similar size of the model in terms of nodes, the thermo-structural analysis was

FIGURE 8 Calculated temperature distribution across the uncoated model of the piston without the cooling gallery.

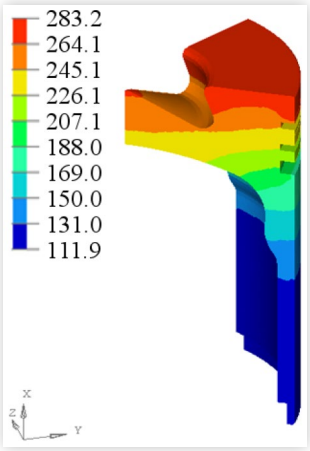

TABLE 12 FE model size and thermo-structural simulation time.

Model	# of nodes	CPU time	Clock time (4 cores)
A	456903	51h 50′ 27″	8h 49′ 25″
B	474722	47h 53′ 39″	9h 01′ 33″

far more time-consuming. This is a consequence of including the previously neglected components, wrist pin and connecting rod (although modeled with first-order elements), and considering the contact behavior. The latter requires to perform a nonlinear static analysis.

The effects of gas pressure, inertial forces, and thermal loads were analyzed both separately and combined to better understand their contributions to the overall stress state.

Gas Pressure Effect The Von Mises stress distributions given by application of the gas pressure alone are shown in Figure 9. For this kind of load, the highest stress is localized at the wrist pin-piston contact, in the upper part of the wrist pin housing. The comparison shows some significant differences in stress: the coating shows higher stresses, especially in the region at the base of the bowl, while the sub-coating region is subjected to lower stresses with respect to the uncoated one. Moreover, the wrist pin housing peak stress is increased by 2.5% for the coated model, since the crown is stiffened by the TBC, and thus the top sector of the pin housing shows a reduced compliance.

Inertial Force Effect Inertial forces depend on mass and acceleration of the system and reach a peak for high rpm becoming dominant with respect to other forces. Their effect is a force in opposite direction with respect to the gas pressure. The analysis pointed out no significant differences in Von Mises stress distribution between coated and uncoated models: in both cases the peak values are concentrated at the bottom of the wrist pin housing, as shown in Figure 10.

Thermal Load Effect Thanks to the high thermal inertia of the materials and to the high speed of the engine cycle, the piston temperature field is substantially constant. Consequently, the same nodal temperatures obtained from the thermal analysis can be used in thermo-structural analysis at any crank angle, which means that the thermal stress and strain will be the same at any point of the engine cycle.

Figure 11 shows the Von Mises stress distribution due to the thermal field alone. The highest stresses are localized in the upper part of the piston and, in particular, around the bowl and in the piston ring region. A considerable peak is reached in the alfin region, since the thermal expansion coefficient of the piston aluminum alloy is almost double than the one of the alfin cast iron. Therefore, the aluminum alloy expansion is contrasted by the cast iron with the result of stress concentrations: tensile stress for the alfin and compression for the piston.

Considering the uncoated piston mode, Figure 11(a), the top land and rigid land surfaces are free to expand under the pressure from the core mass of the piston and are then subjected to tensile stress. On the opposite, the region at the base of the bowl, constrained by the surrounding geometry, is subject to compressive stresses.

FIGURE 9 Von Mises stress distribution (MPa) produced by the gas pressure at TDC for the uncoated (a) and coated (b) piston models.

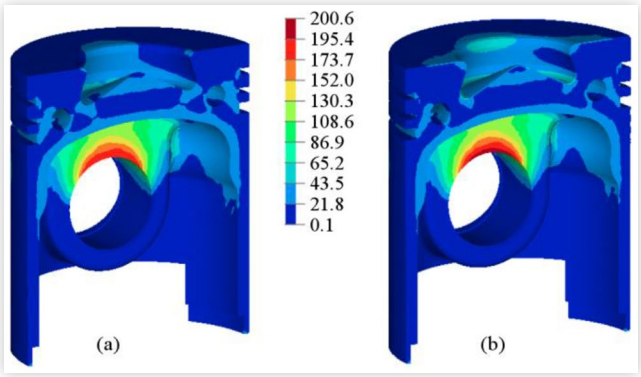

FIGURE 10 Von Mises stress distribution (MPa) produced at TDC by the inertial forces (equal for both coated and uncoated piston models).

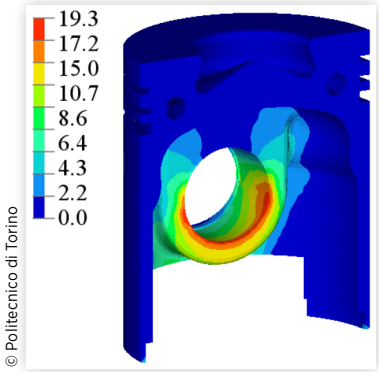

FIGURE 11 Von Mises stress distribution (MPa) produced by the thermal load at TDC for the uncoated (a) and coated (b) piston models.

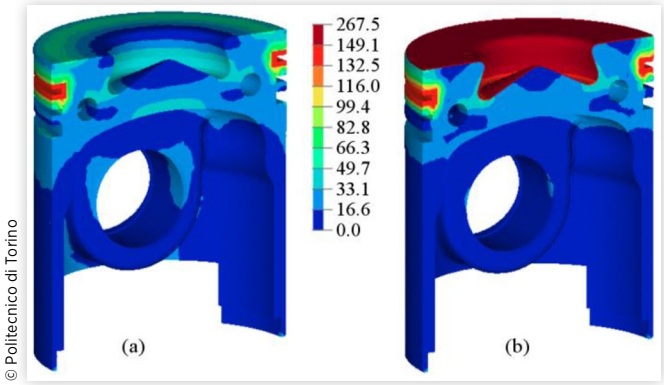

FIGURE 12 Von Mises stress distribution (MPa) produced at TDC by the combined loads for the uncoated (a) and coated (b) piston models.

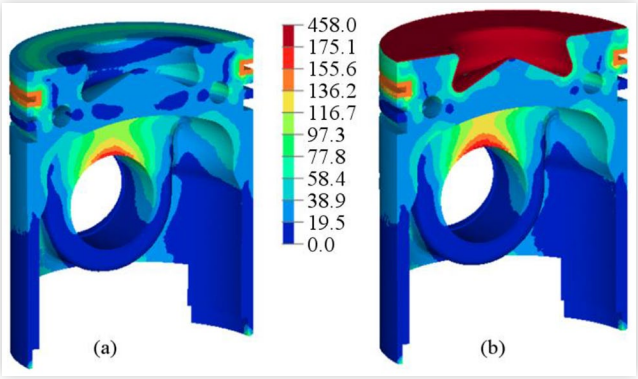

The stress distribution for the coated piston model, Figure 11(b), shows significant changes with respect to the uncoated one. Due to its low expansion coefficient, the TBC acts as a constraint reducing the deformations of the crown. Therefore, the aluminum alloy below the coating is under compression and higher stress concentrations are generated: up to 153 MPa in compression at the alfin interface and 268 MPa in tensile for the coating in the bowl region.

Combined Load Effect The Von Mises stress distributions across the uncoated and coated piston models under the action of combined loads (gas pressure, inertial forces, and thermal loads) are shown in Figure 12, while Figure 13 shows the signed Von Mises distribution. Here, the sign is taken from the principal stress with the largest amplitude to provide a better understanding of the stress conditions. As expected, the thermal load effect is dominant in the upper part of the piston, while the gas pressure load is mainly affecting the wrist pin housing region. These two loads produce effects that mitigate each other since they are opposed: that is, next to the bowl base, the gas pressure produces a tensile stress that is lowered by the compression induced by the thermal load. Also, the upper region of the wrist pin bore is subjected to higher stresses when the gas pressure alone is considered with respect to the case of combined loads.

FIGURE 13 Signed Von Mises stress distribution (MPa) showing tensile/compression regions produced by the combined loads at TDC for the uncoated (a) and coated (b) piston models. The top value of the scale refers to the peak stress in the coating layer, which is hidden to show the stress state of the underlying region.

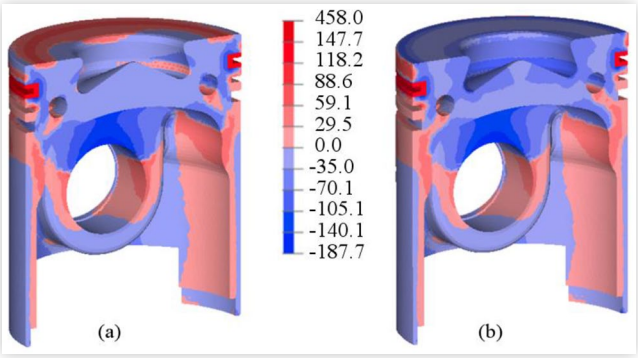

FIGURE 14 Total displacement contour plot of the uncoated (a) and TBC coated (b) piston models at TDC.

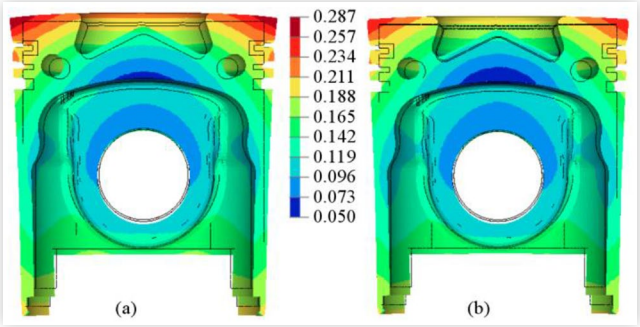

From the signed Von Mises contour plots of Figure 13(b), it is clear the effect of the TBC causes compressive stresses in the underlying aluminum alloy that is subjected to tensile stress in the absence of coating, as reported in Figure 13(a). The nodal displacements resulting in the final deformation of the uncoated and coated piston models are shown in Figure 14.

Tables 13 and 14 summarize the peak stresses for each critical region and compare them to the material yield stress at the reference temperature, to provide the safety factor for the uncoated and coated piston models, respectively. Although the coating introduces higher peak stresses in all regions, the higher thermal insulation provided by the TBC allows for lower local temperature and thus higher yielding stress. As a result, the safety factor is marginally lowered for the wrist pin housing and for the crown regions, and it is the same at the alfin interface.

TABLE 13 Peak stresses and safety factors for the uncoated piston model.

Region	Max Von Mises [MPa]	Material yielding [MPa]	Safety factor
Wrist pin housing	175	190 (160°C)	1.09
Piston crown	60	65 (280°C)	1.08
Alfin interface	115	120 (225°C)	1.04

TABLE 14 Peak stresses and safety factors for the coated piston model.

Region	Max Von Mises [MPa]	Material yield stress [MPa]	Safety factor
Coating	458	560 (300°C)	1.22
Wrist pin housing	188	200 (150°C)	1.06
Piston crown under TBC	83	86 (250°C)	1.04
Alfin interface	125	130 (215°C)	1.04

It can be observed that the coated piston model is subjected to smaller displacements (max. 0.257 mm against 0.287 for the uncoated one), due to both the additional stiffness induced by the TBC and the lower thermal field inside the piston.

Summary/Conclusions

A numerical methodology based on finite element thermo-mechanical analysis was developed to evaluate the effects of TBC on the piston crown for an internal combustion diesel engine. Potential advantages and drawbacks of the coating were discussed based on the available literature. Boundary conditions and relevant material properties were analyzed to reach the highest result accuracy.

First, a thermal analysis has been conducted to evaluate the temperature field across the uncoated and coated piston models. Then, the loads acting on the component were considered both separately and combined to achieve a better understanding of their mutual interaction and of the coating effect on the stress state.

The thermal analysis has pointed out a decrease of temperature up to 40°C in the upper part of the piston for the coated model. The most critical stress for the thermo-mechanical analysis has been identified in the contact region between the wrist pin and the piston bore, as consequence of the gas pressure load. Despite the lower deformations induced by the reduced thermal load, the stiffening effect provided by the TBC results in higher peak stress. However, the lower temperature field inside the piston also implies higher allowable yielding stress for the piston aluminum alloy: as a consequence, the overall safety factor is only marginally affected.

The methodology has been validated by comparison with other numerical data available from the literature. However, further improvements are possible by improving the following aspects:

- A better characterization of the thermal exchange phenomena, eventually involving computational fluid dynamics for considering oil and gas flows around the piston body
- A finer second-order hexahedral mesh to increase the accuracy of the wrist pin-piston contact analysis
- The addition of secondary actions by introducing the liner, the piston rings, and the lubrication condition between them
- The implementation of a transient analysis to account for the whole engine cycle and to better evaluate the effects of the piston motion on its stress state
- The implementation of a fatigue life assessment, by including thermo-structural analysis at different points of the engine cycle and eventually considering lateral forces where not negligible
- A more detailed modeling of the TBC and its substrate to better evaluate the stress at the interface and to assess the coating life in real working conditions

Contact Information

Paolo Baldissera
Politecnico di Torino, corso Duca degli Abruzzi, 24 - 10129 Torino, Italy
paolo.baldissera@polito.it
+39 011 090 6917

Definitions/Abbreviations

α - Thermal expansion coefficient
λ - Thermal conductivity
ν - Poisson's ratio
ρ - Specific weight
$\sigma_{0.1\ true}$ - True yielding stress at 0.1% of plastic deformation
$\sigma_{0.2\ true}$ - True yielding stress at 0.2% of plastic deformation
$\sigma_{R\ true}$ - True rupture stress
c_p - Specific heat capacity
APS - Atmospheric Plasma Spray
E - Elastic modulus
FEM - Finite Element Method
h - Thermal exchange coefficient
LHRE - Low Heat Rejection Engines
T - Temperature
TBC - Thermal Barrier Coating
T_{gas} - Gas temperature
UTS - Ultimate Tensile Strength
VPS - Vacuum Plasma Spray

References

1. Holmberg, K., Andersson, P., and Erdemir, A., "Global Energy Consumption due to Friction in Passenger Cars," *Tribology International* 47:221-234, 2012, doi:10.1016/j.triboint.2011.11.022.
2. Romero, C.A., "Heat Transfer Modeling of a Diesel Engine," Technological University of Pereira, Report 2011, https://www.utp.edu.co/cms-utp/data/bin/UTP/web/uploads/media/comunicaciones/documentos/Heat-Transfer-Modeling-of-a-Diesel-Engine.doc.
3. Borman, G. and Nishiwaki, K., "Internal-Combustion Engine Heat Transfer," *Progress in Energy and Combustion Science* 13(1):1-46, 1987, doi:10.1016/0360-1285(87)90005-0.
4. Heywood, J.B., *Internal Combustion Engine Fundamentals* (1988). ISBN:007028637X.
5. Ahmaniemi, S., Vuoristo, P., Mäntylä, T., Cernuschi, F. et al., "Modified Thick Thermal Barrier Coatings: Thermophysical Characterization," *Journal of the European Ceramic Society* 24(9):2669-2679, 2004, doi:10.1016/j.jeurceramsoc.2003.08.016.

6. Technology, N.R.C. (U. S.). C. on A.D., "A Review of the State of the Art and Projected Technology of Low Heat Rejection Engines: A Report," National Academy Press; Available from Commission on Engineering and Technical Systems National Research Council, Washington, DC, 1987.
7. Shabir, M.F., Authars, S., Ganesan, S., Karthik, R. et al., "Low Heat Rejection Engines - Review," SAE Technical Paper 2010-01-1510, 2010, doi:10.4271/860314.
8. Sivakumar, G. and Senthil Kumar, S., "Investigation on Effect of Yttria Stabilized Zirconia Coated Piston Crown on Performance and Emission Characteristics of a Diesel Engine," *Alexandria Engineering Journal* 53(4):787-794, 2014, doi:10.1016/j.aej.2014.08.003.
9. Morel, T., Wahiduzzaman, S., and Fort, E.F., "Heat Transfer Experiments in an Insulated Diesel Engine," SAE Technical Paper 880186, 1988, doi:10.4271/880186.
10. Morel, T., Wahiduzzaman, S., Fort, E.F., Tree, D.R. et al., "Heat Transfer in a Cooled and an Insulated Diesel Engine," SAE Technical Paper 890572, 1989, doi:10.4271/890572.
11. Cheng, W.K., Wong, V.W., and Gao, F., "Heat Transfer Measurement Comparisons in Insulated and Non-Insulated Diesel Engines," SAE Technical Paper 890570, 1989, doi:10.4271/890570.
12. Assanis, D.N., Friedmann, F.A., Wiese, K.L., Zaluzec, M.J. et al., "A Prototype Thin-Film Thermocouple for Transient Heat Transfer Measurements in Ceramic-Coated Combustion Chambers," SAE Technical Paper 900691, 1990, doi:10.4271/900691.
13. Woschni, G., Spindler, W., and Kolesa, K., "Heat Insulation of Combustion Chamber Walls - A Measure to Decrease the Fuel Consumption of IC Engines?" SAE Technical Paper 870339, 1987, doi:10.4271/870339.
14. Furuhama, S. and Enomoto, Y., "Heat Transfer into Ceramic Combustion Wall of Internal Combustion Engines," SAE Technical Paper 870153, 1987, doi:10.4271/870153.
15. Dickey, D., "The Effect of Insulated Combustion Chamber Surfaces on Direct-Injected Diesel Engine Performance, Emissions and Combustion," SAE Technical Paper 890292, 1989, doi:10.4271/890292.
16. Assanis, D.N., Wiese, K., Schwarz, E., and Bryzik, W., "The Effects of Ceramic Coatings on Diesel Engine Performance and Exhaust Emissions," SAE Technical Paper 910460, 1991, doi:10.4271/910460.
17. Ciniviz, M., Hasimoglu, C., Şahin, F., and Salman, M.S., "Impact of Thermal Barrier Coating Application on the Performance and Emissions of a Turbocharged Diesel Engine," *Proceedings of the Institution of Mechanical Engineers, Part D: Journal of Automobile Engineering* 222(12):2447-2455, 2008, doi:10.1243/09544070JAUTO851.
18. Taymaz, I., "The Effect of Thermal Barrier Coatings on Diesel Engine Performance," *Surface and Coatings Technology* 201(9-11 Spec. Iss.):5249-5252, 2007, doi:10.1016/j.surfcoat.2006.07.123.
19. Büyükkaya, E., Engin, T., and Cerit, M., "Effects of Thermal Barrier Coating on Gas Emissions and Performance of a LHR Engine with Different Injection Timings and Valve Adjustments," *Energy Conversion and Management* 47(9-10):1298-1310, 2006, doi:10.1016/j.enconman.2005.06.021.
20. Wright, P.K. and Evans, A.G., "Mechanisms Governing the Performance of Thermal Barrier Coatings," *Current Opinion in Solid State and Materials Science* 4(3):255-265, 1999, doi:10.1016/S1359-0286(99)00024-8.
21. Hassan, M., "Finite Element Analysis (FEA) Implementation of Thermal Barrier Coating (TBC) Lifetime Prediction Methods," Master's thesis, 2013.
22. Schlichting, K.W., Padture, N.P., and Klemens, P.G., "Thermal Conductivity of Dense and Porous Yttria-Stabilized Zirconia," *Journal of Materials Science* 36(12):3003-3010, 2001, doi:10.1023/A:1017970924312.
23. J.R. Davis & Associates and ASM International; Thermal Spray Society Training Committee, *Handbook of Thermal Spray Technology* (ASM International, 2004). ISBN:0871707950.
24. Wang, H., Dinwiddie, R.B., and Porter, W.D., "Development of a Thermal Transport Database for Air Plasma Sprayed ZrO2-Y2O3 Thermal Barrier Coatings," *Journal of Thermal Spray Technology* 19(5):879-883, 2010, doi:10.1007/s11666-010-9486-z.
25. Qi, H.-Y., Zhou, L.Z., Ma, H.-Q., Yang, X.-G., and Li, X., "In-Situ Measurement of Elastic Modulus for Ceramic Top-Coat at High Temperature," *Journal of Central South University of Technology (English Edition)* 15(Suppl. 2):372-376, 2008, doi:10.1007/s11771-008-0490-0.
26. Fogarassy, P., Rotaru, F., Markocsan, N., and Straumal, B., "Finite Element Analysis of the Bondcoat Influence on Residual Stress during the Plasma Thermal Spraying of Partially Stabilised Zirconia," *Pulverizarea Termica ISIM Timis* 83-92, 2000.
27. Funk, M., Ma, K., Eberl, C., Schoenung, J.M. et al., "High-Temperature Mechanical Behavior of End-of-Life Cryomilled NiCrAlY Bond Coat Materials," *Metallurgical and Materials Transactions A: Physical Metallurgy and Materials Science* 42(8):2233-2241, 2011, doi:10.1007/s11661-011-0659-2.
28. Zhang, H., Xing, J., and Guo, C., "Thermal Analysis of Diesel Engine Piston," *Journal of Chemical and Pharmaceutical Research* 5(9):388-393, 2013.
29. Gehlot, R. and Tripathi, B., "Thermal Analysis of Holes Created on Ceramic Coating for Diesel Engine Piston," *Case Studies in Thermal Engineering* 8:291-299, 2016, doi:10.1016/j.csite.2016.08.008.